energies

MDPI

Article

Stability, Electronic Structure and Thermodynamic Properties of Nanostructured MgH_2 Thin Films

Omar Mounkachi [1,2,*], Asmae Akrouchi [1], Ghassane Tiouitchi [2], Marwan Lakhal [3], Elmehdi Salmani [1], Abdelilah Benyoussef [1,4], Abdelkader Kara [5], Abdellah El Kenz [1], Hamid Ez-Zahraouy [1] and Amine El Moutaouakil [6,*]

1 Laboratory of Condensed Matter and Sciences Interdisciplinary, Faculty of Science, Mohammed V University, Rabat BP 1014, Morocco; akrouchi.asmae@gmail.com (A.A.); salmanielmehdi@gmail.com (E.S.); benyous@fsr.ac.ma (A.B.); akenzele@yahoo.com (A.E.K.); ezahamid@gmail.com (H.E.-Z.)
2 Modeling, Simulation & Data Analysis Program, Mohammed VI Polytechnic University, Ben Guerir 43150, Morocco; t.ghassane@gmail.com
3 Ecole Supérieure de Technologie de Laâyoune, Ibn Zohr University, Laayoune BP 3007, Morocco; lakhal.marwan@gmail.com
4 Hassan II Academy of Sciences and Techniques, Mohammed V University, Rabat BP 1014, Morocco
5 Department of Physics, University of Central Florida, Orlando, FL 32816, USA; Abdelkader.Kara@ucf.edu
6 Department of Electrical and Communication Engineering, College of Engineering, United Arab University, Abu Dhabi, P.O. Box 15551, Al Ain 15551, United Arab Emirates
* Correspondence: omar.mounkachi@fsr.um5.ac.ma (O.M.); a.elmoutaouakil@uaeu.ac.ae (A.E.M.)

Citation: Mounkachi, O.; Akrouchi, A.; Tiouitchi, G.; Lakhal, M.; Salmani, E.; Benyoussef, A.; Kara, A.; El Kenz, A.; Ez-Zahraouy, H.; El Moutaouakil, A. Stability, Electronic Structure and Thermodynamic Properties of Nanostructured MgH_2 Thin Films. *Energies* **2021**, *14*, 7737. https://doi.org/10.3390/en14227737

Academic Editors: Claudia Barolo and Venkata Kamalakar Mutta

Received: 2 October 2021
Accepted: 14 November 2021
Published: 18 November 2021

Abstract: Magnesium is an attractive hydrogen storage candidate due to its high gravimetric and volumetric storage capacities (7.6 wt.% and 110 gH_2/l, respectively). Unfortunately, its use as a storage material for hydrogen is hampered by the high stability of its hydride, its high dissociation temperature of 573–673 K and its slow reaction kinetics. In order to overcome those drawbacks, an important advancement toward controlling the enthalpy and desorption temperatures of nanostructured MgH_2 thin films via stress/strain and size effects is presented in this paper, as the effect of the nano-structuring of the bulk added to a biaxial strain on the hydrogen storage properties has not been previously investigated. Our results show that the formation heat and decomposition temperature correlate with the thin film's thickness and strain/stress effects. The instability created by decreasing the thickness of MgH_2 thin films combined with the stress/strain effects induce a significant enhancement in the hydrogen storage properties of MgH_2.

Keywords: DFT calculations; hydrogen storage; MgH_2 thin films; strain; stress; size

1. Introduction

The development of power storage methods and technologies is considered one of the most important efforts of this decade, in which hydrogen has become an important element among the clean and renewable sources of energy. Its combustion produces around three times more energy compared to fossil fuels and without any greenhouse gas emissions [1]. This has led many researchers and industrialists to consider hydrogen the key to the global energy revolution. Nevertheless, the safe, efficient and secure storage and transportation of this element remain the major obstacles facing its wide use and commercialization. Additionally, there are three technologies available for hydrogen storage, which are storing the gas under high pressure, storing it in liquid form at low temperature or storing it in solid materials. The first two methods have disadvantages relating to the difficulties in forming the two "high pressure and low temperature" conditions. On the other hand, solid materials have recently been used for hydrogen storage by way of hydrogen atoms being absorbed and stored in metallic matrixes, such as intermetallic materials, organic compounds, metal hydrides, porous materials and complex hydrides [2–9].

Due to the increase in interest in the development of hydrogen storage properties, our study focuses on the thermodynamic properties of magnesium hydride (MgH_2) in both its bulk and thin film forms, with or without the application of strain. MgH_2 is one of the most promising materials for hydrogen storage due to its high gravimetric and volumetric capacities (7.65 wt.%, 110 g.H_2/l) and low cost. However, its utilization has been prevented due to its high dissociation temperature, which is much higher than the requirement of the US Department of Energy, and the slow reaction kinetics of this hydride [10–12]. Therefore, different attempts were made in order to improve its abs/desorption properties [13–27]. Theoretically, using first principles calculations, it was found that there is a reduction in stability and temperature of decomposition when Mg is combined with several additives [13–16]. By using Kinetic Monte Carlo simulations, it has been shown that MgH_2 exhibits slow hydrogenation and dehydrogenation kinetics [14]. The addition of small quantities of aluminum and transition metals like Ni, Fe and V can accelerate such kinetics without considerably reducing the associated capacities [14]. Moreover, the single and double substitution of MgH_2 with lightweight elements, namely boron and lithium, show an improvement in the hydrogen storage properties of the substituted MgH_2 with a remarkable increase in its gravimetric and volumetric capacities, which exceed those of the pure one [16]. Recently, the effect of magnesium vacancies in the magnesium hydride (MgH_2) has been investigated. The results reveal that the magnesium vacancies and hydrogen doping have a beneficial effect on the hydrogen storage properties of the hydride by decreasing its desorption temperature and stability and increasing its capacities [28,29].

Today, it is well known that nano-structuring materials, with or without straining, lead to new physical phenomena and/or significant improvement of their physical properties for new and existing applications, ranging from the energy field to the bioelectronic and electronic communication fields [30–45]. The straining of nano-sized silicon (Si), for example, increased the plasma wave nonlinearities inside the channel of a traditional Si-based modulation-doped field-effect transistor, which enhanced the coupling and affinity between the Si channel and the electromagnetic radiation in the Terahertz domain [45]. The same has also been shown for compound semiconductors, such as InGaAs, InP and InAs semiconductors. Another example is the nano-structuring of graphene, MoS_2 and other 2D materials in nanotubes, nanoribbons or quantum dots, which changes the bandgap form and the electronic and optical properties, enabling the use of such materials in many fields, such as biosensing applications (by offering better binding conditions between the nano-structure and the investigated molecules) or Terahertz applications (by providing a tuning dependency between the sizes of the structure and the frequency of operation) [40].

Experimentally, MgH_2-based thin films reportedly showed improved hydrogen desorption performance compared to those of bulk MgH_2 [17–27]. Lu H-B et al. [17] reported that the ΔH of hydrogen absorption and desorption for the bulk Mg/MgH_2 film were significantly high compared to those of the previously prepared 2D nano-structured Mg/MgH_2 film, with values reaching 73.9 ± 0.7 and 77.7 ± 0.8 kJ/mol, respectively. Barawi et al. [18] and Baldi et al. [19] found that the interface effects between the substrate and the Mg film cause the thickness to be an important factor in the hydrogen absorption kinetics of Mg films. Mooij [20] deduced that the energy of the interface can cause destabilization of the phase of MgH_2 at the nanoscale when there is a positive difference in interface energy between MgH_2 and Mg, and causes stabilization in the case of a negative difference. Tao et al. [21] confirmed these findings using the DFT calculations on the dehydrogenation properties of MgH_2/TiH_2 multilayers. Moreover, studies conducted over approximately a decade [22,23] showed that 50–100 nm thick MgH_2-based thin films have reduced stability. Therefore, the enhancement of the dehydrogenation properties of Mg/MgH_2-based nanocomposites undoubtedly depends on the interface misfit and strain energy [24–27]. However, the origins of the kinetic properties and tuned thermodynamics of MgH_2 of different sizes and under strain had not been thoroughly investigated before. In this paper, the properties of the nano-structured MgH_2 thin film and the effect of biaxial strain are investigated using first principles calculations.

2. Computational Methods

In the present work, DFT-based calculations were performed using the QUANTUM ESPRESSO (QE) code [46]. The generalized-gradient approximation—Perdew–Burke–Ernzerhof (GGA-PBE) functional [47] was used, with a plane wave pseudopotential method available in the QE code. The energy cutoff of 40Ry and the k-point meshes for the Brillouin zone integration were cited as being 12 × 12 × 12 and 12 × 12 × 1 for the bulk and thin film of the MgH_2 structure, respectively. Furthermore, the use of the self-consistent criteria of the density and the energy was conducted with 10^{-6} Ry and 10^{-8} Ry of precision, respectively.

In the first step, the structural parameters of the α-MgH_2 structure were taken from the experimental results, where α-MgH_2 crystallized in a rutile structure (space group P42/mnm, No.136) with lattice constants a = b = 4.501 Å and c = 3.010 Å, where 2a (0.0, 0.0, 0.0) and 4f (0.304, 0.304, 0.0) sites were occupied by Mg and H atoms, respectively [48]. Then, the structure was fully relaxed with a force convergence of 10^{-4} Ry/Bohr and an energy convergence of 10^{-7} Ry. Once the unstrained unit cell of the bulk α-MgH_2 was entirely relaxed, the magnesium hydride thin films were modeled by creating 1 × 1 × z supercells of different sizes along the Z direction, ranging from four to seventy-six unit cells. For example, a thin film of a thickness of 22 nm was presented with a 1 × 1 × 76 supercell composed of 308 atoms of magnesium and 154 atoms of hydrogen, while a supercell of 1 × 1 × 4 represented a thin film of 1.2 nm. Periodic boundary conditions were applied along the X and Y directions in order to make these systems infinite in the (X, Y) plane. In addition, a vacuum of 35 Å was used along the Z-direction to isolate the system of layers, as shown in Figure 1.

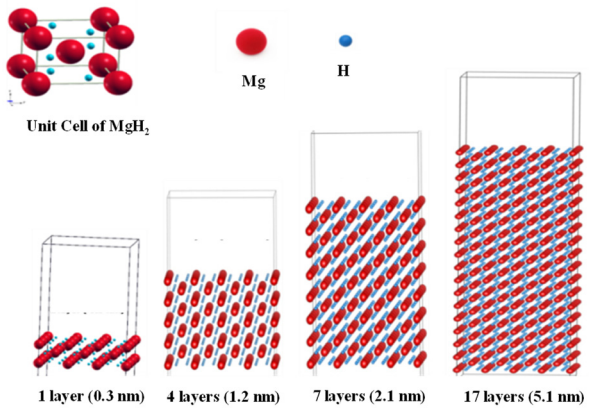

Figure 1. Structures of bulk and different sizes of MgH_2 thin films. (The red spheres are magnesium and the blue ones are hydrogen).

The mechanical stress effect on the storage properties of thin film Mg was evaluated by imposing a mechanical biaxial strain along the [100] and [010] directions on the relaxed MgH_2 (22 nm) thin film according to the following Equation (1) [49–51]:

$$\varepsilon_{xx}(\%) = \varepsilon_{yy}(\%) = \frac{a(b) - a_0(b_0)}{a_0(b_0)} \quad (1)$$

where the lattice constants $a(b)$ of the MgH_2 (22 nm) supercell are restricted to different values ranging from −2.7% to 1.8% with a step of 0.1%, and $a_0(b_0)$ are the equilibrium lattice constants. The "c" parameter is obtained by relaxing atomic positions under each strain. The negative and positive values of ε_{xx} (ε_{yy}) indicate the compression and tensile strain in the x and y axes, respectively.

3. Results and Discussion

3.1. Size-Dependent Thermodynamic Properties

Before studying the properties of thin film MgH_2, the results of the formation enthalpy and desorption temperature of the free strain MgH_2 unit cell are presented. From the relaxation calculations, the lattice parameters for the bulk structure are a = b = 4.520 Å and c = 3.010 Å, which are close to the reported theoretical values [13–16,49] and the experimental ones [48]. The heat of formation for this material was calculated from Equation (2):

$$\Delta H = E_{tot}(MgH_2) - E_{tot}(Mg) - E_{tot}(H_2) \quad (2)$$

where E_{tot} (MgH_2), E_{tot} (Mg) and E_{tot} (H_2) are the total energies of magnesium hydride, magnesium and molecular hydrogen, respectively. The total energies of the various components were first calculated by using the Plane-Wave Self-Consistent Field (PWSCF) method, and then the heat of formation was deduced using Equation (2).

The desorption temperature can be estimated from Equation (3):

$$T_{des} = -\frac{\Delta H}{\Delta S} \quad (3)$$

where the entropy is considered to be equivalent to $\Delta S \approx \Delta S(H_2)$ = 130.7 J/mol.K, which corresponds to the entropy change due to a mole of gas changing to the solid form [52,53]. The different results and energy values are listed in Table 1.

Table 1. Energies, formation heat and desorption temperature.

	Energies (eV)	**ΔH (eV/H_2)**	**T_{des} (K)**
Mg (hcp)	−3.07	_	_
H_2	−6.60	_	_
Mg (22 nm)	−235.84	_	_
MgH_2 (bulk)	−17.74	−0.74	542.87
MgH_2 (22 nm)	−1362.37	−0.56	414.75

The calculated enthalpy of formation and desorption temperature of the bulk MgH_2 are −0.74 eV/H_2 and 542 K, respectively, which is in good agreement with previous DFT calculations and experimental results [17,54–56]. The magnesium hydride provides a better stability and a high desorption temperature that are much higher than US-DOE requirements [17]. To improve the hydrogen storage properties of this compound, the nano-structuring effect on the thermodynamic properties and hydrogen storage capacities of the MgH_2 structure was investigated by studying the size dependent hydrogen desorption in Mg hydride thin films with different thicknesses: 1 nm, 4 nm, 5 nm and 22 nm (Figure 1). To do so, the total energies of Mg thin films, hydrogen molecules and MgH_2 thin films are calculated first (see Table 1). Subsequently, the heat formation can be deduced using Equation (4) for the thin film model and the corresponding desorption temperature by using Equation (3):

$$\Delta H = E_{tot}(MgH_2)nano - E_{tot}(Mg)nano - \frac{n}{2}E_{tot}(H_2) \quad (4)$$

where n is the number of H atoms contained in the MgH_2 thin film. The effect of the size of MgH_2 on the desorption temperatures and enthalpy of formation are shown in Figure 2.

By reducing the size, a significant enhancement in the heat of formation is observed from −0.74 eV/H_2 for the bulk to −0.515 eV/H_2 for the thin film of 1-nm thickness. This improvement is accompanied by a significant reduction of desorption temperature from 542 K to 380 K. The last value is in the optimum range 289–393 K for the practical use of fuel cell vehicles [15].

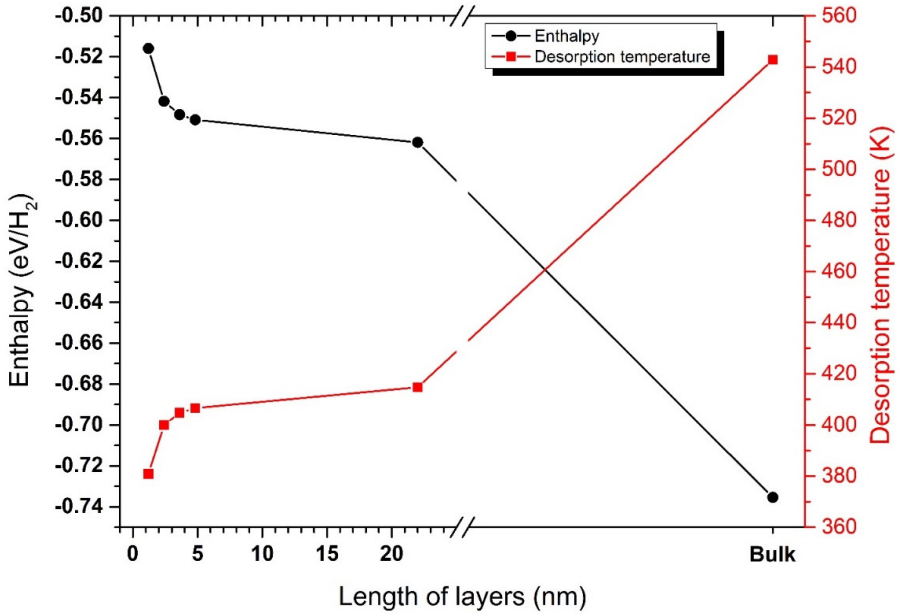

Figure 2. Variation of desorption temperatures and enthalpy vs. thickness of MgH_2.

These results are in line with the reported findings [18,21,55,57], which confirm that the size change on MgH_2 films improves the thermodynamic properties of this compound, owing to the surface properties and the thickness of the 2D nano-structured film. On the other hand, the stability of the MgH_2 thin film was improved compared to other reported works [57–59] by reducing the thickness of the thin film to 1 nm. Additionally, to describe the effect of size on the hydrogen storage capacities of MgH_2, the gravimetric and volumetric capacities for bulk and different sizes of MgH_2 thin film are calculated and presented in Figure 3. Firstly, the storage capacities of MgH_2 bulk is in good agreement with the values of another study [55]. The obtained results show that MgH_2 has high gravimetric 7.66 wt.% and volumetric 110.14 g.H_2/l capacities. Secondly, the results show that the volumetric capacity increases from bulk to thin film thickness, whereas the gravimetric capacity remains the same, which indicates that the nano-structuration has a positive effect on the storage capacities.

Assuming that the desorption behavior of the thin films is along the Z axis, it is necessary to aim for nanometer sizes for thin layers in order to have an efficient hydrogen storage medium. The remaining axes (X, Y) were reserved for the application of stress on MgH_2 thin films of 22 nm thickness in order to investigate the effect of such stress on de/hydrogenation properties, as described in the next section.

3.2. Strained MgH_2 Thin Film Properties

By reducing the size, we observed a significant enhancement in both the heat of formation and the desorption temperature from −0.74 eV/H_2 and 542 K, respectively, for the bulk to −0.515 eV/H_2 and 380 K, respectively, for the thin film of 1 nm thickness. These results are in good agreement with the reported findings of previously published works [18,55,57], which confirm that the nano-structuring applied in this work by changing the size of MgH_2 films improves the thermodynamic properties of this compound.

In order to simulate the extrinsic effect of the stresses, which can be observed experimentally by the mismatch, a biaxial tensile/compressive strain is applied to the 22 nm thin film along the [100] and [010] directions according to Equation (1). In this case, the lattice constants "a" and "b" of the 22 nm thin supercell are constrained to strain values ranging from 4.4 Å to 4.6 Å, which correspond to a strain varying from −2.7% to 1.8%, as shown in Figures 4–6.

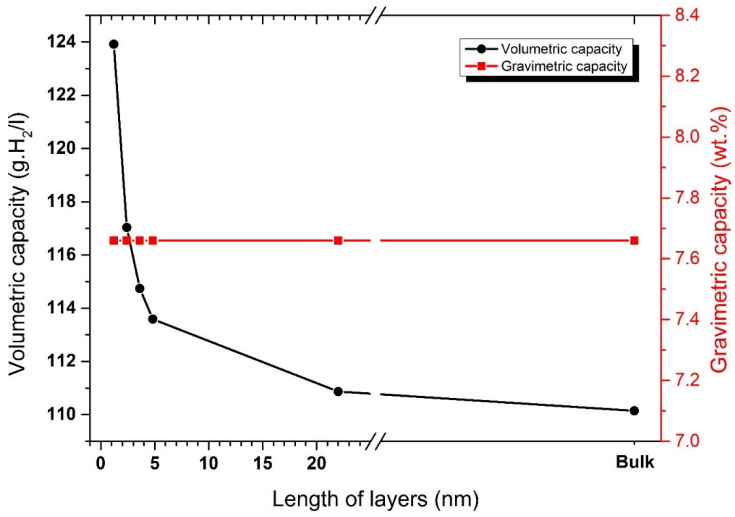

Figure 3. Variation of volumetric and gravimetric capacities vs. thickness of MgH_2.

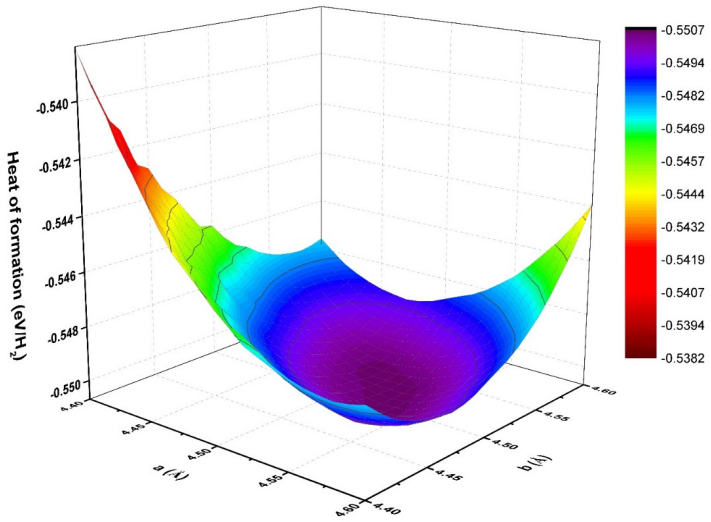

Figure 4. The effect of stress (variation of lattices "a" and "b") on the stability of MgH_2 thin film (thickness: 22 nm).

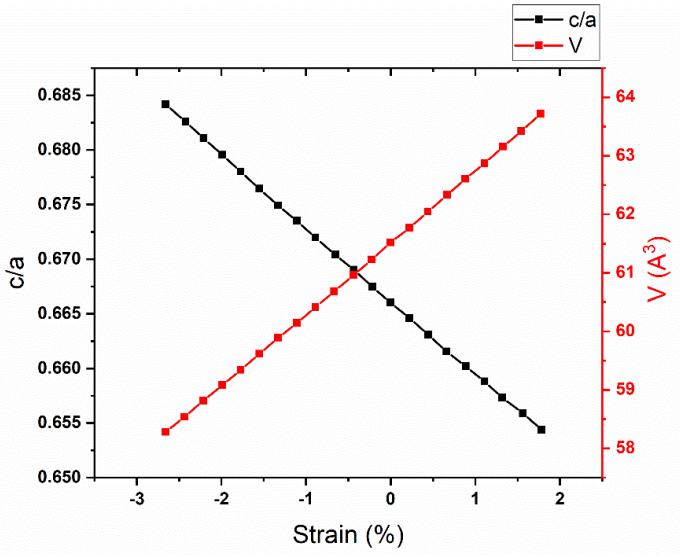

Figure 5. The ratio c/a and supercell volume V as a function of biaxial strain ε in MgH_2 thin film.

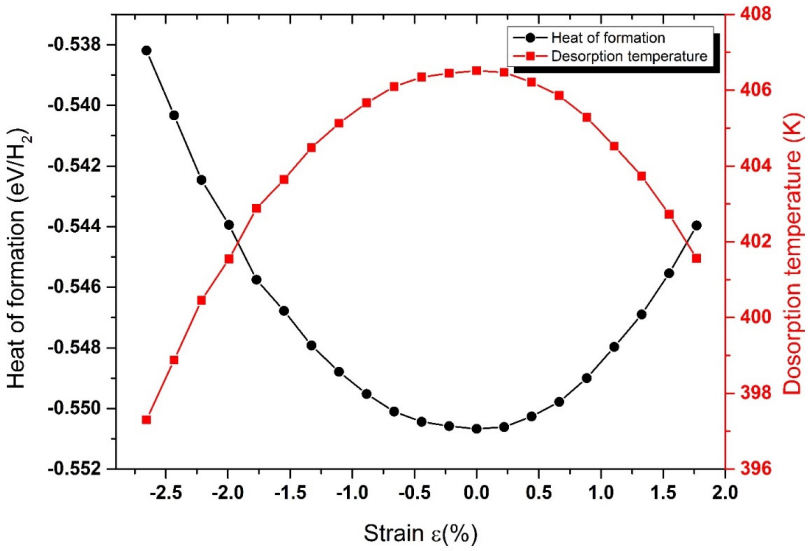

Figure 6. Formation enthalpies and desorption temperatures as a function of strain ε.

Figure 4 shows the stability of a MgH_2 (22 nm) thin film system under strain. The maximum stability is found for the relaxed parameters, and this stability is reduced considerably when we apply the strain. Moreover, the lattice constant "c" increases under biaxial compressive strain, while it decreases under the tensile one. In other words, under biaxial compressive strain, the lattice constant of the MgH_2 thin film along the *z*-axis direction is elongated, which results in an increasing ratio of c/a relative to that (0.667) of the strain-free state, as shown in Figure 5. The maximal ratio of c/a reaches 0.684 at the compressive strain of −2.7%. Comparatively, the lattice along the *z*-axis direction of the nano-structured MgH_2 shrinks under biaxial tensile strain, yielding a decreasing ratio of c/a relative to that of the strain-free state. A minimum of 0.654 is obtained at the tensile strain of +1.8%. Meanwhile, MgH_2 expands or contracts under biaxial tensile or compressive strain and its cell volume increases or decreases nearly linearly compared to the magnitude of strain as shown in Figure 5. Therefore, it can be derived that either biaxial tensile or compressive strain is likely to cause structural deformation of the MgH_2 crystal, or its lattice distortion becomes severe with the increasing magnitude of biaxial strain.

The effect of strain on the thermodynamic properties of MgH_2 thin films (with a thickness of 22 nm) is summarized in Figure 6. This figure shows that the application of strain on MgH_2 thin film systems reduces their stability compared to that of strain-free ones, which improves their desorption temperatures.

This can be understood as follows: in the case of compressive strain, the distance between atoms is too small; this can lead to a strong interaction and therefore reduces the stability of the system. On the other hand, the H atoms can diffuse easily when we apply a tensile strain, and this consequently reduces the stability of the MgH_2 thin film with 22 nm of thickness.

The obtained results are partially comparable to the ones found by J. Zhang [49], who states that the strain lowers the decomposition temperature and the stability of the bulk MgH_2. Furthermore, the reported variation of formation enthalpy and decomposition temperature observed in the case of compressive strain are totally different than those of the tensile one, whereas in our work, both strains (compressive and tensile) symmetrically increase the enthalpy formation and decrease the desorption temperature for strained MgH_2 (22 nm) thin film relative to the free strain. The finding's behaviors are similar to the results of H. Benzidi et al. [60], who showed that $LiBH_4$ free of strain leads to a high stability, while compressive or biaxial tensile strain lowers the stability of the $LiBH_4$ structure. Finally, due to the contribution of strain, the stability and the decomposition temperature for strained MgH_2 (22 nm) thin film are reduced compared to those of the strain-free system, which is a great enhancement of MgH_2 storage properties. The calculation results of this

study show that T_{des} decreases significantly when increasing the magnitude of strain to a value equal to 398 K, which is close to the optimum range 289–393 K for the practical use of proton-exchange membrane fuel cells (PEMFC) [57].

In conclusion, the nano-structuring of the bulk and the addition of biaxial strain resulted in a beneficial improvement to the storage properties of MgH_2.

4. Conclusions

In the present paper, the hydrogen storage performances of MgH_2 thin films were studied through the investigation of the effect of size and strain on the thermodynamic properties using first principles DFT calculations implemented in the Quantum-espresso package. Firstly, the studied thermodynamic properties of the bulk MgH_2 present a high stability of -0.74 eV/H_2 and a high decomposition temperature of 542.87 K, which is in good agreement with other theoretical and experimental results. Secondly, the nano-structured MgH_2 thin film improves the thermodynamic properties of the bulk MgH_2 considerably when the decomposition temperature and the stability of the MgH_2 thin film can be reduced to 380 K and -0.515 eV/H_2, respectively, by reducing its thickness to 1 nm. Finally, in addition to the effect of size, the hydrogen storage properties of MgH_2 (22 nm) thin film were improved by applying a biaxial strain on this system, which caused the stability and the decomposition temperature of the MgH_2 (22 nm) thin film to be reduced from -0.56 eV/H_2 and 414.75 K to -0.539 eV/H_2 and 398 K, respectively, before and after strain. This is a great enhancement of MgH_2 storage properties, even though the strain effect on the thermodynamic properties of the MgH_2 thin film has not been studied previously.

Author Contributions: A.E.M. and O.M. conceived/planned the simulations and supervised the findings of this work. A.A., G.T. and M.L. contributed to the configuration of the models. M.L., E.S., A.B., A.K., A.E.K. and H.E.-Z. verified the results and contributed to the interpretation of results. M.L., A.E.M. and O.M. wrote the manuscript with insights from all the authors. A.E.M. secured the funds for this research. All authors discussed the results and contributed to the final manuscript. All authors have read and agreed to the published version of the manuscript.

Funding: This research was partly funded by United Arab Emirates University UPAR project, grant number 31N393.

Institutional Review Board Statement: Not applicable.

Informed Consent Statement: Not applicable.

Conflicts of Interest: The authors declare no conflict of interest.

References

1. Züttel, A.; Remhof, A.; Borgschulte, A.; Friedrichs, O. Hydrogen: The Future Energy Carrier. *Philos. Trans. R. Soc. A Math. Phys. Eng. Sci.* **2010**, *368*, 3329–3342. [CrossRef] [PubMed]
2. Schlapbach, L.; Züttel, A. Hydrogen-Storage Materials for Mobile Applications. *Nature* **2001**, *414*, 353–358. [CrossRef] [PubMed]
3. Gross, A.F.; Vajo, J.J.; Van Atta, S.L.; Olson, G.L. Enhanced Hydrogen Storage Kinetics of LiBH4 in Nanoporous Carbon Scaffolds. *J. Phys. Chem. C* **2008**, *112*, 5651–5657. [CrossRef]
4. Hartman, M.R.; Rush, J.J.; Udovic, T.J.; Bowman, R.C.; Hwang, S.-J. Structure and Vibrational Dynamics of Isotopically Labeled Lithium Borohydride Using Neutron Diffraction and Spectroscopy. *J. Solid State Chem.* **2007**, *180*, 1298–1305. [CrossRef]
5. Bellosta von Colbe, J.; Ares, J.-R.; Barale, J.; Baricco, M.; Buckley, C.; Capurso, G.; Gallandat, N.; Grant, D.M.; Guzik, M.N.; Jacob, I.; et al. Application of Hydrides in Hydrogen Storage and Compression: Achievements, Outlook and Perspectives. *Int. J. Hydrogen Energy* **2019**, *44*, 7780–7808. [CrossRef]
6. Zhang, L.; Zheng, J.; Xiao, X.; Wang, X.; Huang, X.; Liu, M.; Wang, Q.; Chen, L. A New Strategy to Remarkably Improve the Low-Temperature Reversible Hydrogen Desorption Performances of LiBH4 by Compositing with Fluorographene. *Int. J. Hydrogen Energy* **2017**, *42*, 20046–20055. [CrossRef]
7. Shao, J.; Xiao, X.; Fan, X.; Zhang, L.; Li, S.; Ge, H.; Wang, Q.; Chen, L. Low-Temperature Reversible Hydrogen Storage Properties of LiBH4: A Synergetic Effect of Nanoconfinement and Nanocatalysis. *J. Phys. Chem. C* **2014**, *118*, 11252–11260. [CrossRef]
8. Liu, Y.; Pan, H. *New and Future Developments in Catalysis: Batteries Hydrogen Storage and Fuel Cells*; Elsevier: Amsterdam, The Netherlands, 2013; pp. 377–405.
9. Chen, P. *Comprehensive Renewable Energy*; Elsevier: Amsterdam, The Netherlands, 2012; pp. 157–177.

10. Song, M.Y.; Kwon, S.N.; Park, H.R.; Hong, S.-H. Improvement in the Hydrogen Storage Properties of Mg by Mechanical Grinding with Ni, Fe and V under H_2 Atmosphere. *Int. J. Hydrogen Energy* **2011**, *36*, 13587–13594. [CrossRef]
11. Sakintuna, B.; Lamari-Darkrim, F.; Hirscher, M. Metal Hydride Materials for Solid Hydrogen Storage: A Review. *Int. J. Hydrogen Energy* **2007**, *32*, 1121–1140. [CrossRef]
12. Léon, A.; Knystautas, E.J.; Huot, J.; Schulz, R. Hydrogenation Characteristics of Air-Exposed Magnesium Films. *J. Alloys Compd.* **2002**, *345*, 158–166. [CrossRef]
13. Bhihi, M.; Lakhal, M.; Naji, S.; Labrim, H.; Belhaj, A.; Benyoussef, A.; Kenz, A.E.; Loulidi, M.; Khalil, B.; Mounkachi, O.; et al. First Principle Calculations for Improving Desorption Temperature in Mg 16 H 32 Doped with Ca, Sr and Ba Elements. *Bull. Mater. Sci.* **2014**, *37*, 1731–1736. [CrossRef]
14. Lakhal, M.; Bhihi, M.; Benyoussef, A.; El Kenz, A.; Loulidi, M.; Naji, S. The Hydrogen Ab/Desorption Kinetic Properties of Doped Magnesium Hydride MgH_2 Systems by First Principles Calculations and Kinetic Monte Carlo Simulations. *Int. J. Hydrogen Energy* **2015**, *40*, 6137–6144. [CrossRef]
15. Bhihi, M.; El Khatabi, M.; Lakhal, M.; Naji, S.; Labrim, H.; Benyoussef, A.; El Kenz, A.; Loulidi, M. First Principle Study of Hydrogen Storage in Doubly Substituted Mg Based Hydrides. *Int. J. Hydrogen Energy* **2015**, *40*, 8356–8361. [CrossRef]
16. Abdellaoui, M.; Lakhal, M.; Bhihi, M.; El Khatabi, M.; Benyoussef, A.; El Kenz, A.; Loulidi, M. First Principle Study of Hydrogen Storage in Doubly Substituted Mg Based Hydrides Mg5MH12 (M = B, Li) and Mg4BLiH12. *Int. J. Hydrogen Energy* **2016**, *41*, 20908–20913. [CrossRef]
17. Lu, H.B.; Poh, C.K.; Zhang, L.C.; Guo, Z.P.; Yu, X.B.; Liu, H.K. Dehydrogenation Characteristics of Ti- and Ni/Ti-Catalyzed Mg Hydrides. *J. Alloys Compd.* **2009**, *481*, 152–155. [CrossRef]
18. Barawi, M.; Granero, C.; Díaz-Chao, P.; Manzano, C.V.; Martin-Gonzalez, M.; Jimenez-Rey, D.; Ferrer, I.J.; Ares, J.R.; Fernández, J.F.; Sánchez, C. Thermal Decomposition of Non-Catalysed MgH_2 Films. *Int. J. Hydrogen Energy* **2014**, *39*, 9865–9870. [CrossRef]
19. Baldi, A.; Palmisano, V.; Gonzalez-Silveira, M.; Pivak, Y.; Slaman, M.; Schreuders, H.; Dam, B.; Griessen, R. Quasifree Mg–H Thin Films. *Appl. Phys. Lett.* **2009**, *95*, 071903. [CrossRef]
20. Mooij, L.P.A.; Baldi, A.; Boelsma, C.; Shen, K.; Wagemaker, M.; Pivak, Y.; Schreuders, H.; Griessen, R.; Dam, B. Interface Energy Controlled Thermodynamics of Nanoscale Metal Hydrides. *Adv. Energy Mater.* **2011**, *1*, 754–758. [CrossRef]
21. Tao, S.-X.; Notten, P.H.L.; van Santen, R.A.; Jansen, A.P.J. Dehydrogenation Properties of Epitaxial (100) MgH_2/TiH_2 Multilayers—A DFT Study. *Comput. Mater. Sci.* **2011**, *50*, 2960–2966. [CrossRef]
22. Yoshimura, K.; Yamada, Y.; Okada, M. Hydrogenation of Pd Capped Mg Thin Films at Room Temperature. *Surf. Sci.* **2004**, *566–568*, 751–754. [CrossRef]
23. Oguchi, H.; Tan, Z.; Heilweil, E.J.; Bendersky, L.A. In-Situ Infrared Imaging Methodology for Measuring Heterogeneous Growth Process of a Hydride Phase. *Int. J. Hydrogen Energy* **2010**, *35*, 1296–1299. [CrossRef]
24. Hydrogen Storage and Structure Variation in Mg/Pd Multi-Layer Film. *J. Alloys Compd.* **2010**, *504*, 493–497. [CrossRef]
25. Pereira, V.M.; Castro Neto, A.H. Strain Engineering of Graphene's Electronic Structure. *Phys. Rev. Lett.* **2009**, *103*, 046801. [CrossRef]
26. Mandal, T. Strain Induced Phase Transition in CdSe Nanowires: Effect of Size and Temperature. *Appl. Phys. Lett.* **2012**, *101*, 021906. [CrossRef]
27. Lu, J.; Choi, Y.J.; Fang, Z.Z.; Sohn, H.Y.; Rönnebro, E. Hydrogen Storage Properties of Nanosized MgH_2–$0.1TiH_2$ Prepared by Ultrahigh-Energy−High-Pressure Milling. *J. Am. Chem. Soc.* **2009**, *131*, 15843–15852. [CrossRef] [PubMed]
28. Bahou, S.; Labrim, H.; Lakhal, M.; Bhihi, M.; Hartiti, B.; Ez-Zahraouy, H. Improving Desorption Temperature and Kinetic Properties in MgH_2 by Vacancy Defects: DFT Study. *Int. J. Hydrogen Energy* **2020**, *45*, 10806–10813. [CrossRef]
29. Bahou, S.; Labrim, H.; Lakhal, M.; Bhihi, M.; Hartiti, B.; Ez-Zahraouy, H. Magnesium Vacancies and Hydrogen Doping in MgH_2 for Improving Gravimetric Capacity and Desorption Temperature. *Int. J. Hydrogen Energy* **2021**, *46*, 2322–2329. [CrossRef]
30. Samy, O.; Zeng, S.; Birowosuto, M.D.; El Moutaouakil, A. A Review on MoS_2 Properties, Synthesis, Sensing Applications and Challenges. *Crystals* **2021**, *11*, 355. [CrossRef]
31. Samy, O.; Birowosuto, D.; El Moutaouakil, A. A Short Review on Molybdenum Disulfide (MoS_2) Applications and Challenges. In Proceedings of the 2021 6th International Conference on Renewable Energy: Generation and Applications (ICREGA), Al Ain, United Arab Emirates, 2–4 February 2021; pp. 220–222.
32. Samy, O.; El Moutaouakil, A. A Review on MoS2 Energy Applications: Recent Developments and Challenges. *Energies* **2021**, *14*, 4586. [CrossRef]
33. Tiouitchi, G.; Ali, M.A.; Benyoussef, A.; Hamedoun, M.; Lachgar, A.; Kara, A.; Ennaoui, A.; Mahmoud, A.; Boschini, F.; Oughaddou, H.; et al. Efficient Production of Few-Layer Black Phosphorus by Liquid-Phase Exfoliation. *R. Soc. Open Sci.* **2020**, *7*, 201210. [CrossRef]
34. Abed, J.; Rajput, N.S.; Moutaouakil, A.E.; Jouiad, M. Recent Advances in the Design of Plasmonic Au/TiO_2 Nanostructures for Enhanced Photocatalytic Water Splitting. *Nanomaterials* **2020**, *10*, 2260. [CrossRef] [PubMed]
35. Moutaouakil, A.E.; Kang, H.-C.; Handa, H.; Fukidome, H.; Suemitsu, T.; Sano, E.; Suemitsu, M.; Otsuji, T. Room Temperature Logic Inverter on Epitaxial Graphene-on-Silicon Device. *Jpn. J. Appl. Phys.* **2011**, *50*, 070113. [CrossRef]
36. Moutaouakil, A.E. Two-Dimensional Electronic Materials for Terahertz Applications: Linking the Physical Properties with Engineering Expertise. In Proceedings of the 2018 6th International Renewable and Sustainable Energy Conference (IRSEC), Rabat, Morocco, 5–8 December 2018; pp. 1–4.

37. Moutaouakil, A.E.; Suemitsu, T.; Otsuji, T.; Coquillat, D.; Knap, W. Nonresonant Detection of Terahertz Radiation in High-Electron-Mobility Transistor Structure Using InAlAs/InGaAs/InP Material Systems at Room Temperature. *J. Nanosci. Nanotechnol.* **2012**, *12*, 6737–6740. [CrossRef]
38. Moutaouakil, A.E.; Komori, T.; Horiike, K.; Suemitsu, T.; Otsuji, T. Room Temperature Intense Terahertz Emission from a Dual Grating Gate Plasmon-Resonant Emitter Using InAlAs/InGaAs/InP Material Systems. *IEICE Trans. Electron.* **2010**, *93*, 1286–1289. [CrossRef]
39. El Moutaouakil, A.; Suemitsu, T.; Otsuji, T.; Videlier, H.; Boubanga-Tombet, S.-A.; Coquillat, D.; Knap, W. Device Loading Effect on Nonresonant Detection of Terahertz Radiation in Dual Grating Gate Plasmon-Resonant Structure Using InGaP/InGaAs/GaAs Material Systems. *Phys. Status Solidi C* **2011**, *8*, 346–348. [CrossRef]
40. Hijazi, A.; Moutaouakil, A.E. Graphene and MoS2 Structures for THz Applications. In Proceedings of the 2019 44th International Conference on Infrared, Millimeter, and Terahertz Waves (IRMMW-THz), Paris, France, 1–6 September 2019; pp. 1–2.
41. Moutaouakil, A.E.; Fukidome, H.; Otsuji, T. Investigation of Terahertz Properties in Graphene Ribbons. In Proceedings of the 2020 45th International Conference on Infrared, Millimeter, and Terahertz Waves (IRMMW-THz), Buffalo, NY, USA, 8–13 November 2020; pp. 1–2.
42. El Moutaouakil, A.; Al Ahmad, M.; Soopy, A.K.K.; Najar, A. Porous Silicon NWs with FiTC-Doped Silica Nanoparticles. In Proceedings of the 2021 6th International Conference on Renewable Energy: Generation and Applications (ICREGA), Al Ain, United Arab Emirates, 2–4 February 2021; pp. 6–8.
43. Moutaouakil, A.E.; Watanabe, T.; Haibo, C.; Komori, T.; Nishimura, T.; Suemitsu, T.; Otsuji, T. Spectral Narrowing of Terahertz Emission from Super-Grating Dual-Gate Plasmon-Resonant High-Electron Mobility Transistors. *J. Phys. Conf. Ser.* **2009**, *193*, 012068. [CrossRef]
44. Moutaouakil, A.E.; Suemitsu, T.; Otsuji, T.; Coquillat, D.; Knap, W. Room Temperature Terahertz Detection in High-Electron-Mobility Transistor Structure Using InAlAs/InGaAs/InP Material Systems. In Proceedings of the 35th International Conference on Infrared, Millimeter, and Terahertz Waves, Rome, Italy, 5–10 September 2010; pp. 1–2.
45. Meziani, Y.M.; Garcia, E.; Velazquez, E.; Diez, E.; El Moutaouakil, A.; Otsuji, T.; Fobelets, K. Strained Silicon Modulation Field-Effect Transistor as a New Sensor of Terahertz Radiation. *Semicond. Sci. Technol.* **2011**, *26*, 105006. [CrossRef]
46. Giannozzi, P.; Baroni, S.; Bonini, N.; Calandra, M.; Car, R.; Cavazzoni, C.; Ceresoli, D.; Chiarotti, G.L.; Cococcioni, M.; Dabo, I.; et al. Quantum Espresso: A Modular and Open-Source Software Project for Quantum Simulations of Materials. *J. Phys. Condens. Matter* **2009**, *21*, 395502. [CrossRef] [PubMed]
47. Perdew, J.P.; Burke, K.; Ernzerhof, M. Generalized Gradient Approximation Made Simple. *Phys. Rev. Lett.* **1996**, *77*, 3865–3868. [CrossRef] [PubMed]
48. Bortz, M.; Bertheville, B.; Böttger, G.; Yvon, K. Structure of the High Pressure Phase γ-MgH_2 by Neutron Powder Diffraction. *J. Alloys Compd.* **1999**, *287*, L4–L6. [CrossRef]
49. Zhang, J.; Zhou, Y.C.; Ma, Z.S.; Sun, L.Q.; Peng, P. Strain Effect on Structural and Dehydrogenation Properties of MgH_2 Hydride from First-Principles Calculations. *Int. J. Hydrogen Energy* **2013**, *38*, 3661–3669. [CrossRef]
50. Tang, J.-L.; Zhu, J.; Qin, W.-F.; Xiong, J.; Li, Y.-R. Structure and Dielectric Characteristics of Epitaxially Strained $BaTiO_3$ Thin Films. *J. Mater. Sci. Mater. Electron.* **2008**, *19*, 466–470. [CrossRef]
51. Benzidi, H.; Lakhal, M.; Benyoussef, A.; Hamedoun, M.; Loulidi, M.; El Kenz, A.; Mounkachi, O. First Principle Study of Strain Effect on Structural and Dehydrogenation Properties of Complex Hydride LiBH4. *Int. J. Hydrogen Energy* **2017**, *42*, 19481–19486. [CrossRef]
52. Nakamura, H.; Nguyen-Manh, D.; Pettifor, D.G. Electronic Structure and Energetics of $LaNi_5$, α-$La_2Ni_{10}H$ and β-$La_2Ni_{10}H_{14}$. *J. Alloys Compd.* **1998**, *281*, 81–91. [CrossRef]
53. Alapati, S.V.; Johnson, J.K.; Sholl, D.S. Identification of Destabilized Metal Hydrides for Hydrogen Storage Using First Principles Calculations. *J. Phys. Chem. B* **2006**, *110*, 8769–8776. [CrossRef] [PubMed]
54. Novaković, N.; Grbović Novaković, J.; Matović, L.; Manasijević, M.; Radisavljević, I.; Paskaš Mamula, B.; Ivanović, N. Ab Initio Calculations of MgH_2, MgH_2:Ti and MgH_2:Co Compounds. *Int. J. Hydrogen Energy* **2010**, *35*, 598–608. [CrossRef]
55. Jain, I.P.; Lal, C.; Jain, A. Hydrogen Storage in Mg: A Most Promising Material. *Int. J. Hydrogen Energy* **2010**, *35*, 5133–5144. [CrossRef]
56. Majidi, R. Density Functional Idea Study of Magnesium Hydride Nano Clusters. *J. Appl. Chim. Res.* **2011**, *19*, 58–65.
57. Sadhasivam, T.; Kim, H.-T.; Jung, S.; Roh, S.-H.; Park, J.-H.; Jung, H.-Y. Dimensional Effects of Nanostructured Mg/MgH_2 for Hydrogen Storage Applications: A Review. *Renew. Sustain. Energy Rev.* **2017**, *72*, 523–534. [CrossRef]
58. Tan, Z.; Chiu, C.; Heilweil, E.J.; Bendersky, L.A. Thermodynamics, Kinetics and Microstructural Evolution during Hydrogenation of Iron-Doped Magnesium Thin Films. *Int. J. Hydrogen Energy* **2011**, *36*, 9702–9713. [CrossRef]
59. Sadhasivam, T.; Sterlin Leo Hudson, M.; Pandey, S.K.; Bhatnagar, A.; Singh, M.K.; Gurunathan, K.; Srivastava, O.N. Effects of Nano Size Mischmetal and Its Oxide on Improving the Hydrogen Sorption Behaviour of MgH_2. *Int. J. Hydrogen Energy* **2013**, *38*, 7353–7362. [CrossRef]
60. Benzidi, H.; Mounkachi, O.; Lakhal, M.; Benyoussef, A.; El Kenz, A. Compression Effect on Electronic Properties and Hydrogen Desroption of LiBH4: First Principal Study. In Proceedings of the 2016 International Renewable and Sustainable Energy Conference (IRSEC), Marrakech, Morocco, 14–17 November 2016; pp. 568–570.